Femtosecond control of electric currents in metallic ferromagnetic heterostructures

T. J. Huisman[1], R. V. Mikhaylovskiy[1], J. D. Costa[2,3], F. Freimuth[4], E. Paz[2], J. Ventura[3], P. P. Freitas[2], S. Blügel[4], Y. Mokrousov[4], Th. Rasing[1] and A. V. Kimel[1]

[1]*Radboud University, Institute for Molecules and Materials, 6525 AJ Nijmegen, The Netherlands.*
[2]*International Iberian Nanotechnology Laboratory, INL, Braga, Portugal.*
[3]*IN-IFIMUP, Rua do Campo Alegre, 687, 4169-007 Porto, Portugal.*
[4]*Peter Grünberg Institut and Institute for Advanced Simulation, Forschungszentrum Jülich and JARA, 52425 Jülich, Germany.*

The idea to utilize not only the charge but also the spin of electrons in the operation of electronic devices has led to the development of spintronics, causing a revolution in how information is stored and processed. A novel advancement would be to develop ultrafast spintronics using femtosecond laser pulses. Employing terahertz (10^{12} Hz) emission spectroscopy and exploiting spin-orbit interaction, we demonstrate optical generation of electric photocurrents in metallic ferromagnetic heterostructures at the femtosecond timescale. The direction of the photocurrent is controlled by the helicity of the circularly polarized light. These results open up new opportunities for realizing spintronics in the unprecedented terahertz regime and provide new insights in all-optical control of magnetism.

Despite the fact that the generation of electrical photocurrents with the help of spin-orbit interaction and circularly polarized light has been demonstrated in noncentrosymmetric semiconductors [1], an application of this concept to metallic materials which are commonly used in spintronic devices has not yet been realized. Helicity dependent photocurrents can be induced due to the Rashba effect [1], which is one of the microscopic mechanisms representing the coupling between the momentum and spin of an electron [2]. This spin-orbit interaction of the conduction electrons in a system characterized by a lack of space inversion symmetry leads to a breaking of the degeneracy between spin-up and spin-down electron sub-bands in momentum space [3-7]. The Rashba effect can be responsible for the phenomenon of spin-orbit torque, when an electric current flowing through a magnetic conductor induces a torque acting on its magnetization $\mathbf{M}$ and tilts it [8-11]. The phenomenon when a tilting magnetization produces an electric current can be seen as an inverse effect. On the other hand, it has been shown that due to the non-dissipative inverse Faraday effect [12,13] or due to the dissipative optical spin transfer torque effect [14], circularly polarized light can induce a tilt to the magnetization. The direction in which the magnetization is tilted is given by $[\mathbf{M}\times\boldsymbol{\sigma}]$, where $\boldsymbol{\sigma}$ is the axial unit vector pointing parallel or antiparallel to the propagation of light depending on its helicity. Hence if a femtosecond circularly polarized optical excitation acts on the magnetization as an effective magnetic field inducing a torque, it should also produce an electrical current mediated by the Rashba effect. The direction of this current is controlled by the helicity of the incident light. However, despite the fact that various helicity dependent ultrafast effects of light on magnetization have been reported [15-17], the strength of these effects in pure metals is still unknown. As a result, the significance of helicity-dependent photocurrents in metallic materials is a priori not obvious.

Although transition ferromagnetic metals do possess space inversion symmetry, effective symmetry breaking can be present at the interfaces between different metals. Interface sensitive magneto-optics [18,19] and the formation of chiral spin structures at the surfaces and interfaces [20-22] are typical examples of magnetic phenomena originating from the spontaneous symmetry breaking at the interfaces of otherwise centrosymmetric metals. For an inverse spin-orbit torque, the resulting current is perpendicular to both the light-induced magnetization and the direction in which the space inversion symmetry is broken $\mathbf{n}$. In particular, in metallic heterostructures with in-plane structural isotropy and in-plane magnetization, one can anticipate the existence of an interfacial in-plane photocurrent generated by circular polarized light as

$$\mathbf{j} = \chi \mathbf{n} \times [\mathbf{M} \times \boldsymbol{\sigma}] I \qquad (1)$$

where χ is a scalar, $\mathbf{n}$ is a polar unit vector normal to the interface and I is the intensity envelope of a circularly-polarized light pulse which exerts a torque on the magnetization and thereby tilts it in plane, see Fig. 1a. A similar equation for the helicity dependent photocurrents can be derived phenomenologically by assuming that the symmetry of our heterostructure is $C_{\infty v}$ [23]. This photo-induced current does not rely on laser-induced heating, contrary to all previous demonstrations of laser-induced spin-currents in metallic heterostructures [24-28].

Symmetry of the terahertz emission from the heterostructures

For our experiments we studied heterostructures made of a single metallic ferromagnetic (FM) layer and a single metallic non-magnetic (NM) layer deposited on a 0.5 mm thick glass substrate. The structures are very similar to those commonly studied in spintronics related research [4,11,27,29-32]. The FM layer chosen here is a 10 nm thick Co film. The main set of the measurements were performed for the heterostructure with a 2 nm thick Pt NM layer. Supporting experiments were performed using heterostructures in which the NM layer was a 2 nm thick Ru, Ta, Au or Cu layer. Additional measurements were performed on a 10 nm thick Co film, with either 1.3, 2.6 or 3.9 nm thick Pt NM layer. We also fabricated a 12 and 30 nm thick Co sample without NM layer and a 2 nm thick Pt sample without FM layer, which acted as references.

The geometry of the experiment is shown in Fig. 1a. To demonstrate the generation and control of the photocurrents, we employ femtosecond circularly polarized laser pulses with a pulse width of 50 fs and a central wavelength of 800 nm. Note that all our experiments are performed at room temperature. According to the Maxwell equations, any sub-picosecond current pulse in the plane of the heterostructure should act as an emitter of electromagnetic radiation in the THz spectral range, polarized parallel to the direction of the current [27], as we also derived in the supplementary information section 1. We detect the electric field of this THz radiation as a probe for the generated currents. A similar experimental approach has been employed to generate and observe electrical photocurrents in semiconductors lacking bulk inversion symmetry [33]. Further details of the experimental procedure can be found in the Methods section. The set of unit vectors **x**, **y** and **z** represents the chosen coordinate system. The incident laser pulses propagate along **z**, the magnetization is parallel to **y** and the *x* and *y* components of the electric field of the emitted THz radiation are detected. We make use of wiregrid polarizers to separately measure the THz emission polarized along the *x*- and *y*-axis.

Note that femtosecond laser-induced emission of the THz radiation polarized perpendicularly with respect to the magnetization, i.e. along **x**, has been reported for similar samples before [27]. The origin of this emission was assigned to electric currents emerging due to the inverse Spin-Hall effect acting on the spin current launched as a result of the ultrafast laser-induced heating of the ferromagnetic metal. As the direction of this spin current is defined by the sample structure and magnetization, no dependence of the corresponding THz emission on the pump polarization was reported in [27] or observed by us. From Eq. (1), as well as from considering the Landau-Lifshitz equation (see section 2 of the supplementary information), it is seen that the helicity dependent laser-induced current is launched parallel to the magnetization $\mathbf{M}$, i.e. along the *y*-axis. Although a laser-induced increase of the electronic temperature is practically unavoidable, the generation of the helicity dependent current theoretically does not require any heating. Aiming to demonstrate the helicity-dependent femtosecond photocurrents, we address our attention to the laser-induced THz emission polarized along **y**.

Figure 1b shows time traces of the *y*-component of the pump-induced THz emission for opposite helicities of the pump light. The time-traces were obtained by performing the measurements at a

magnetic field of B=0.1 Tesla. The figure clearly shows that the electric field of the emitted THz radiation changes sign upon reversal of the helicity. Fig. 1c shows that the emitted electric field also changes sign upon magnetic field reversal. We found that the emission is still present after a reduction of the applied magnetic field to zero, demonstrating a hysteretic behavior.

To reveal the role of the symmetry breaking in the helicity dependent THz generation process, we performed the measurements for two orientations of the sample by rotating the heterostructure around the magnetization over 180^o so that the sign of the polar vector **n** is reversed. Figure 2 shows that this rotation leads to a change in the sign of the emitted helicity dependent THz radiation. The apparent change in delay and timescale of the dynamics upon turning the sample stems from the different propagation of THz radiation and pump light at the wavelength of 800 nm through the glass substrate. Note that the observation of the role of the symmetry breaking in the THz generation indicates that the emitter must be of electric-dipole origin, rather than of magnetic-dipole origin, as the former lacks space-inversion symmetry, while the latter does not.

Different capping layers and fluence dependence

We also studied the laser-induced THz emission from the other samples. The detected values of the helicity dependent emission are summarized in table 1 (see also section 3 of the supplementary information). This table shows that in order to obtain an intense helicity dependent THz emission, Co must be brought in contact with a material with a strong spin-orbit interaction, like Pt. Helicity dependent THz radiation is emitted even for 12 and 30 nm thick films of pure Co. In section 3 of the supplementary information we show that this emission is also sensitive to the symmetry breaking in agreement with Eq. (1). The lack of an adjacent layer with strong spin-orbit interaction makes the radiation from pure Co weak. The relatively low emission from the Co/Au sample can at least partly be related to the high conductivity of the Au layer. The even weaker THz emission from the Co/Cu heterostructure is in line with the negligible spin-orbit interaction of Cu and due to the absorption of the radiation in the Cu layer.

	E_y, odd in helicity of the pump (V/cm)	E_x, pump polarization independent (V/cm)	E_y/E_x
Co(12)	0.09	3.7	0.02
Co(30)	0.13	3.8	0.034
Co(10)/Cu(2)	<0.02	2.7	<0.007
Co(10)/Ta(2)	1.2	9.9	0.12
Co(10)/Ru(2)	1.3	15	0.087
Co(10)/Au(2)	0.3	36	0.0083
Co(10)/Pt(2)	3.5	53	0.066
Co(10)/Pt(1.3)	3.5	23	0.15
Co(10)/Pt(2.6)	3.6	81	0.044
Co(10)/Pt(3.9)	4.1	101	0.041
Pt(2)	<0.02	<0.06	-

Table 1: Observed maximum amplitudes of emitted electric field. The values between brackets indicate the nominal growing thickness of the layers in nanometers. The values in the table are shown for emission polarized parallel to the *y*-axis (helicity dependent) and parallel to the *x*-axis (polarization independent). The values are for the pump light incident from the side of the substrate. The noise of E_y is mainly limited by background noise which is up to 0.02 V/cm. The noise of E_x is mainly limited by the intensity noise of the laser, which results in an uncertainty proportional to the emission amplitude of approximately 0.8%.

To emphasize that the observed helicity dependent THz emission (E_y) is fundamentally different from polarization independent THz emission (E_x) discussed in Ref. [27] (see also section 4 of the supplementary information), we show in table 1 that there is no fixed ratio between their amplitudes

for the different samples. Moreover, the polarization-dependent (E_y) and polarization-independent (E_x) THz emission depend differently on the thickness of the Pt-layer, see Fig. 3a. It is seen that the helicity dependent emission polarized along the *y*-axis hardly varies with varying thickness of the Pt capping layer, which supports the idea that this emission is generated at the interface of the heterostructure. Moreover, Fig. 3b shows that the electric field of the helicity dependent emission scales nearly linearly for low fluences of the laser, with a saturating behavior for increasing fluence. This is in agreement with Eq. (1), taking into account that laser-induced heating is unavoidable and results in a conductivity change as well as a decrease in magnetization (see also section 5 of the supplementary information). Both of these effects can contribute to the saturation behavior shown in Fig. 3b. Thereby, the fact that the electrons are excited far above the Fermi level can also affect the efficiency of a spin-orbit-interaction mechanism and may therefore also contribute to the saturation. The observed fluence dependence shows that the helicity dependent emission does not require a two-fold action of the laser light. For example, one can exclude a scenario in which light first generates a heat driven spin-polarized current directed into the capping layer and subsequently tilts this current in the capping layer by a helicity-driven effect. Such a scenario would result in a super-linear intensity dependence of the THz emission.

Quantifying the photocurrent and effective optomagnetic field

All our experiments indicate that the emitted THz radiation is in full qualitative agreement with the phenomenology of an interfacial helicity-dependent femtosecond photocurrent as expressed in Eq. (1). In order to estimate the amplitude of the observed photocurrent, using the Maxwell equations we derived how the photocurrent from Eq. (1) is related to the electric field of the observed terahertz radiation in our spectrometer (see supplementary information section 1). Our estimate gives that the photocurrent rises on a time-scale of approximately 330 fs with a peak amplitude of the order of 10^9 A/m^2. Note that in order to come to this estimate, we assumed the current to be localized in a 0.5 nm thick interface region between the two different metal layers. However, in reality the thickness in which the current is localized can be larger, and this likely leads to an overestimation of the current density. Also, the spectral bandwidth of the observed THz pulses are comparable to the one of our spectrometer and therefore the bandwidth of the actual dynamics may be broader. Hence the mentioned rise time of 330 fs should also be regarded as an upper bound and the actual dynamics takes place on a time scale between 50 and 330 fs. The experimental bandwidth, and therefore the time resolution, may be improved by using a different type of non-linear electro-opic crystal (e.g. GaP) for detecting the THz radiation. However, increasing the bandwidth of the THz spectrometers leads to a reduction of the signal-to-noise ratio due to the smaller electro-optic coefficient of such crystals.

The results reported above show that the observed phenomenon obeys Eq. (1) and indicate sensitivity to the spin-orbit interaction at the contact of the magnetic and non-magnetic layer. All these results are in agreement with an inverse spin-orbit torque model. Such a model may provide an estimate for the light induced effective magnetic field, which is found to be 0.2 Tesla for the Co (10 nm)/Pt (2 nm) heterostructure (see section 6 of the supplementary information). We note that a light-induced effective magnetic field has indeed been recently confirmed in a similar heterostructure [34].

Implications

The demonstrated ultrafast generation and control of currents at the interfaces of magnetic multilayers opens up intriguing opportunities for fundamental studies of spintronics and magnetic recording. In spintronic devices the direction of the current can be controlled by both voltage and magnetic field. Here we show that the direction of sub-picosecond current pulses can be changed contact-less, without applying a voltage, but by changing the helicity of light. Taking into account the recent advances in focusing circularly polarized light into sub-100 nm areas [35,36], our discovery enables to push fundamental studies of nanospintronics into the THz frequency domain. We also

believe that our observation may pave a way towards understanding all-optical magnetization reversal, boosting future magnetic recording technology. The mechanisms of the recently demonstrated all-optical helicity dependent magnetic switching in Co/Pt heterostructures [16] have already become a subject of intense debates. However, in the models explaining the switching, the roles of the spin-orbit interaction and symmetry breaking are often ignored. We show that adding a thin capping layer with a strong spin-orbit interaction to Co results in significant enhancement of the helicity-dependent response of the heterostructures to an ultrafast optical excitation.

References

1. Ganichev, S.D. et al. Spin-galvanic effect. *Nature* **417**, 153 (2002)
2. Bychkov, Y.A. & Rashba, É.I. Properties of a 2D electron gas with lifted spectral degeneracy. *JETP Letters* **39**, 78 (1984)
3. Chernyshov, A. et al. Evidence for reversible control of magnetization in a ferromagnetic material by means of spin-orbit magnetic field. *Nature Phys.* **5**, 656 (2009)
4. Miron, I. M. et al. Perpendicular switching of a single ferromagnetic layer induced by in-plane current injection. *Nature* **476**, 189 (2011)
5. Freimuth, F., Blügel, S. & Mokrousov, Y. Spin-orbit torques in Co/Pt(111) and Mn/W(001) magnetic bilayers from first principles. *Phys. Rev. B* **90**, 174423 (2014)
6. Kurebayashi, H. et al. An antidamping spin-orbit torque originating from the Berry curvature. *Nature Nanotech.* **9**, 211 (2014)
7. Ciccarelli, C. et al. Magnonic charge pumping via spin-orbit coupling. *Nature Nanotech.* **10**, 50 (2015)
8. Bernevig, B.A. & Vafek, O. Piezo-magnetoelectric effects in p-doped semiconductors. *Phys. Rev. B* **72**, 033203 (2005)
9. Manchon, A. & Zhang, S. Theory of spin torque due to spin-orbit coupling. *Phys. Rev. B* **79**, 094422 (2009)
10. Brataas, A., Kent, A.D. & Ohno, H. Current-induced torques in magnetic materials. *Nature Mater.* **11**, 372 (2012)
11. Garello, K. et al. Symmetry and magnitude of spin-orbit torques in ferromagnetic heterostructures. *Nature Nanotech.* **8**, 587 (2013)
12. Pershan, P.S., van der Ziel, J.P. & Malmstrom, L.D. Theoretical Discussion of the Inverse Faraday Effect, Raman Scattering, and Related Phenomena. *Phys. Rev.* **143**, 574 (1966)
13. Kimel, A.V. et al. Ultrafast non-thermal control of magnetization by instantaneous photomagnetic pulses. *Nature* **435**, 655 (2005)
14. Němec, P. et al. Experimental observation of the optical spin transfer torque. *Nature Phys.* **8**, 411 (2012)
15. Stanciu, C.D. et al. All-Optical Magnetic Recording with Circularly Polarized Light. *Phys. Rev. Lett.* **99**, 047601 (2007)
16. Lambert, C.H. et al. All-optical control of ferromagnetic thin films and nanostructures. *Science* **345**, 1337 (2014)
17. Mangin, S. et al. Engineered materials for all-optical helicity-dependent magnetic switching. *Nature Mater.* **13**, 286 (2014)
18. Koopmans, B., Groot Koerkamp, M., Rasing, Th. & Van den Berg, H. Observation of Large Kerr Angles in the Nonlinear Optical Response from Magnetic Multilayers. *Phys. Rev. Lett.* **74**, 3692 (1995)
19. Wierenga, H.A. et al. Interface Magnetism and Possible Quantum Well Oscillations in Ultrathin Co/Cu Films Observed by Magnetization Induced Second Harmonic Generation. *Phys. Rev. Lett.* **74**, 1462 (1995)
20. Romming, N. et al. Writing and Deleting Single Magnetic Skyrmions. *Science* **341**, 636 (2013)
21. Dupé, B., Hoffmann, M., Paillard, C. & Heinze, S. Tailoring magnetic skyrmions in ultra-thin transition metal films. *Nature Commun.* **5**, 1038 (2014)
22. Pyatakov, A.P. & Zvezdin, A.K. Dzyaloshinskii-Moriya-type interaction and Lifshitz invariant in Rashba 2D electron gas systems. *EPL* **107**, 67002 (2014)
23. Weber, W. et al. Magneto-gyrotropic photogalvanic effects in GaN/AlGaN two-dimensional systems. *Solid State Commun.* **145**, 56 (2008)
24. Malinowski, G. et al. Control of speed and efficiency of ultrafast demagnetization by direct transfer of spin angular momentum. *Nature Phys.* **4**, 855 (2008)
25. Melnikov, A. et al. Ultrafast Transport of Laser-Excited Spin-Polarized Carriers in Au/Fe/Mgo(001). *Phys. Rev. Lett.* **107**, 076601 (2011)
26. Rudolf, D. et al. Ultrafast magnetization enhancement in metallic multilayers driven by superdiffusive spin current. *Nature Commun.* **3**, 1037 (2012)
27. Kampfrath, T. et al. Terahertz spin current pulses controlled by magnetic heterostructures. *Nature Nanotech.* **8**, 256 (2013)
28. Choi, G.-M., Min, B.-C., Lee, K.-J. & Cahill, D.G. Spin current generated by thermally driven ultrafast demagnetization. *Nature Commun.* **5**, 4334 (2014)
29. Mosendz, O. et al. Quantifying Spin Hall Angles from Spin Pumping: Experiments and Theory. *Phys. Rev. Lett.* **104**, 046601 (2010)
30. Liu, L. et al. Spin-Torque Switching with the Giant Spin Hall Effect of Tantalum. *Science* **336**, 555 (2012)

31. Kim, J. et al. Layer thickness dependence of the current-induced effective field vector in Ta|CoFeB | MgO. *Nature Mater.* **12**, 240 (2013)
32. Rojas-Sánchez, J.-C. et al. Spin Pumping and Inverse Spin Hall Effect in Platinum: The Essential Role of Spin-Memory Loss at Metallic Interfaces. *Phys. Rev. Lett.* **112**, 106602 (2014)
33. Schleicher, J.M., Harrel, S.M. & Schmuttenmaer, C.A. Effect of spin-polarized electrons on terahertz emission from phoexcited GaAs. *J. Appl. Phys.* **105**, 113116 (2009)
34. Choi, G.-M. *Ultrafast Laser Driven Spin Generation in Metallic Ferromagnets*. Doctoral Dissertation (2015)
35. Drezet, A., Genet, C. & Ebbesen, T.W. Miniature Plasmonic Wave Plates. *Phys. Rev. Lett.* **101**, 043902 (2008)
36. Biagioni, P. et al. Near-field polarization shaping by a near-resonant plasmonic cross antenna. *Phys. Rev. B* **80**, 153409 (2009)

Acknowldegments
We would like to thank T. Toonen, A. van Etteger and S. Semin for technical support. We would like to thank A. Brataas, A. Kirilyuk, A.K. Zvezdin and V.V. Bel'kov for fruitful discussions. This work was supported by the Foundation for Fundamental Research on Matter (FOM), the European Unions Seventh Framework Program (FP7/2007-2013) grant No. 280555 (Go-Fast) and No. 281043 (FemtoSpin), Projects No. Norte-070124-FEDER-000070 and FEDER-POCTI/0155, European Research Council grant No. 257280 (Femtomagnetism) and grant No. 339813 (Exchange), and the program "Leading Scientist" of the Russian Ministry of Education and Science (14.Z50.31.0034). J.D.C. is thankful for FCT grant SFRH/BD/7939/2011.

Contributions
T.J.H., R.V.M., J.D.C. and A.V.K. conceived the experiments. T.J.H. and R.V.M. designed and built the experimental set up. T.J.H. performed the measurements and analysed the data with help of R.V.M. and A.V.K.. J.D.C. fabricated and characterized the samples with help of E.P., J.V., and P.P.F. The theoretical formalisms were derived by T.J.H., R.V.M. and F.F. with contributions from Y.M., S.B. and A.V.K.. T.J.H., R.V.M, F.F, and A.V.K. co-wrote the paper. All authors discussed the results and commented on the manuscript. The project was coordinated by A.V.K..

Competing financial interests
The authors declare no competing financial interests.

Corresponding author
Correspondence to T.J. Huisman

Figure captions

Figure 1: Experimental schematics and symmetry of the emitted THz radiation. a Layered structure under study and the scheme of the experiment. A magnetic field B=0.1 Tesla is applied in-plane along the *y*-axis to saturate the magnetization **M**. **b** Electric field of the emitted radiation polarized along the *y*-axis as a function of time measured for the opposite helicities of light. **c** The emitted radiation changes sign with magnetization. The position of zero time is arbitrarily chosen.

Figure 2: The role of the symmetry breaking directionality for the THz emission in Co (10 nm)/Pt (2 nm). The shown THz emission is odd with respect to the helicity and the magnetization $E_{y,odd}=(E_y(\sigma+,M+)-E_y(\sigma+,M-)-E_y(\sigma-,M+)+E_y(\sigma-,M-))/4$. **a** Electric field of the emitted radiation when the pump is incident from the side of the substrate. **b** The same as panel **a** but for the case when the pump is incident from the side of the Pt layer. The apparent change in delay and timescale of dynamics when reversing the sample stems from different propagation of THz radiation and light at the wavelength of 800 nm through the substrate. The position of zero time is arbitrary chosen, but kept consistent between the measurements.

Figure 3: Amplitude of the THz emission as function of the thickness of the Pt capping layer and fluence. a Amplitude of the helicity dependent (E_y) and independent (E_x) emission as function of the

Pt capping layer thickness. The Pt capping layers are deposited on a 10 nm thick Co film. **b** Helicity dependent electric field as function of fluence for when the pump is incident from the side of the substrate (n+) and Pt layer (n-). The solid lines are linear regressions, which serve to guide the eye.

Methods

Materials. The metallic films were deposited on a 0.5 mm thick glass substrate using an ultrahigh vacuum multitarget sputtering system, with a base pressure of $5 \cdot 10^{-8}$ Torr. For the metallic heterostructures a 10 nm thick ferromagnetic layer of Co was deposited, capped with a non-magnetic layer of Pt, Au, Ru, Ta or Cu. As references we also deposited a single layer of 12 and 30 nm thick Co on a glass substrate and a single layer of 2 nm Pt on a glass substrate. Additionally we created Co/Pt samples with a Pt thickness of 1.3, 2.6 and 3.9 nm. For each material the deposition conditions, i.e. applied current and Argon gas flux were optimized to achieve the best quality and reproducibility of the films. All films were deposited with a deposition rate smaller than 1 angstrom per second for a good control of the thickness. During deposition the samples are rotated to ensure uniformity of the films. After deposition the samples were exposed to air. X-ray reflectivity measurements were performed by a PanAnalytical X Pert PRO MRD system with a wavelength of λ = 0.154 nm, allowing to estimate the roughness of the layers and the interfaces. For the Co(10)/Pt(2) sample we extracted a roughness of 0.4 nm between the substrate and Co, and 1 nm between the Pt and the Co layers.

Experimental setup. The experimental setup is comparable to the one we used in [37,38]. An intense laser pulse with a duration of 50 fs and a fluence of approximately 1 mJ/cm^2, the pump, is incident on the metallic films with a spot diameter of 1 mm, inducing rapid changes to the magnetization and to the electronic transport properties. According to the Maxwell equations, these dynamics give rise to emission of radiation in the terahertz (THz) spectral range, which can be detected as a probe of these dynamics. This THz radiation propagates first through two wiregrid polarizers, used to measure its polarization. These polarizers have a transmission higher than 95% in a range of 0 to 2 THz and have an extinction ratio for an electric field at 1 THz of $2 \cdot 10^3$, enabling to separate the THz radiation polarized along the *x*- and *y*-axis. Subsequently, the emission is collected and refocused using two gold coated parabolic mirrors. The radiation is focused onto a ZnTe crystal which is simultaneously gated by pulses from the laser. The electric field of the THz radiation induces birefringence by means of the Pockels effect inside the ZnTe crystal, causing additional ellipticity of the gating laser pulses. Measuring this ellipticity with a balanced bridge detection scheme provides the amplitude of the electric field of the emitted THz radiation.

The magnetization dynamics can also be observed using the magneto-optical Kerr effect (MOKE) detected with a weak laser pulse, the probe. This probe are pulses from the laser with a fluence ten times smaller than that of the pump. While the pump is incident normal to the sample, the probe is incident under an angle of 25^o, allowing for spatial separation of the reflected beams. The initially linear polarized probe is measured after reflection on the sample polarization resolved with a balanced bridge detection scheme.

Methods References

37. Mikhaylovskiy, R.V. et al. Ultrafast modification of exchange interactions in iron oxides. *Nature Commun.* **6**, 8190 (2015)
38. Huisman, T.J., Mikhaylovskiy, R.V., Tsukamoto, A., Rasing, Th. & Kimel, A.V. Simultaneous measurements of terahertz emission and magneto-optical Kerr effect for resolving ultrafast laser-induced demagnetization dynamics. *Phys. Rev. B* **92**, 104419 (2015)

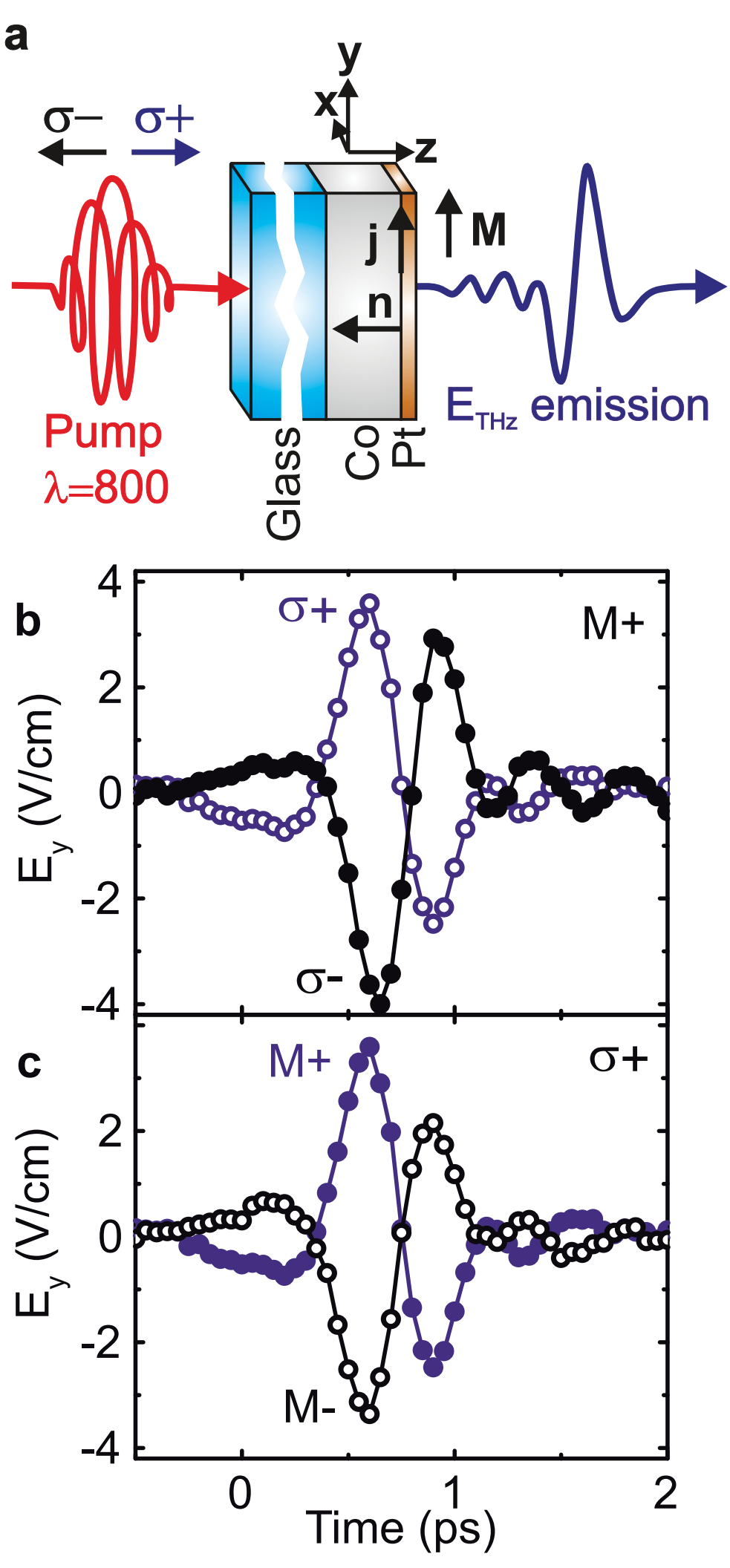
a
σ−
σ+
y
x
z
j
n
M
Pump
λ=800
Glass
Co
Pt
E_THz emission
b
σ+
M+
σ-
E_y (V/cm)
c
M+
σ+
M-
E_y (V/cm)
Time (ps)

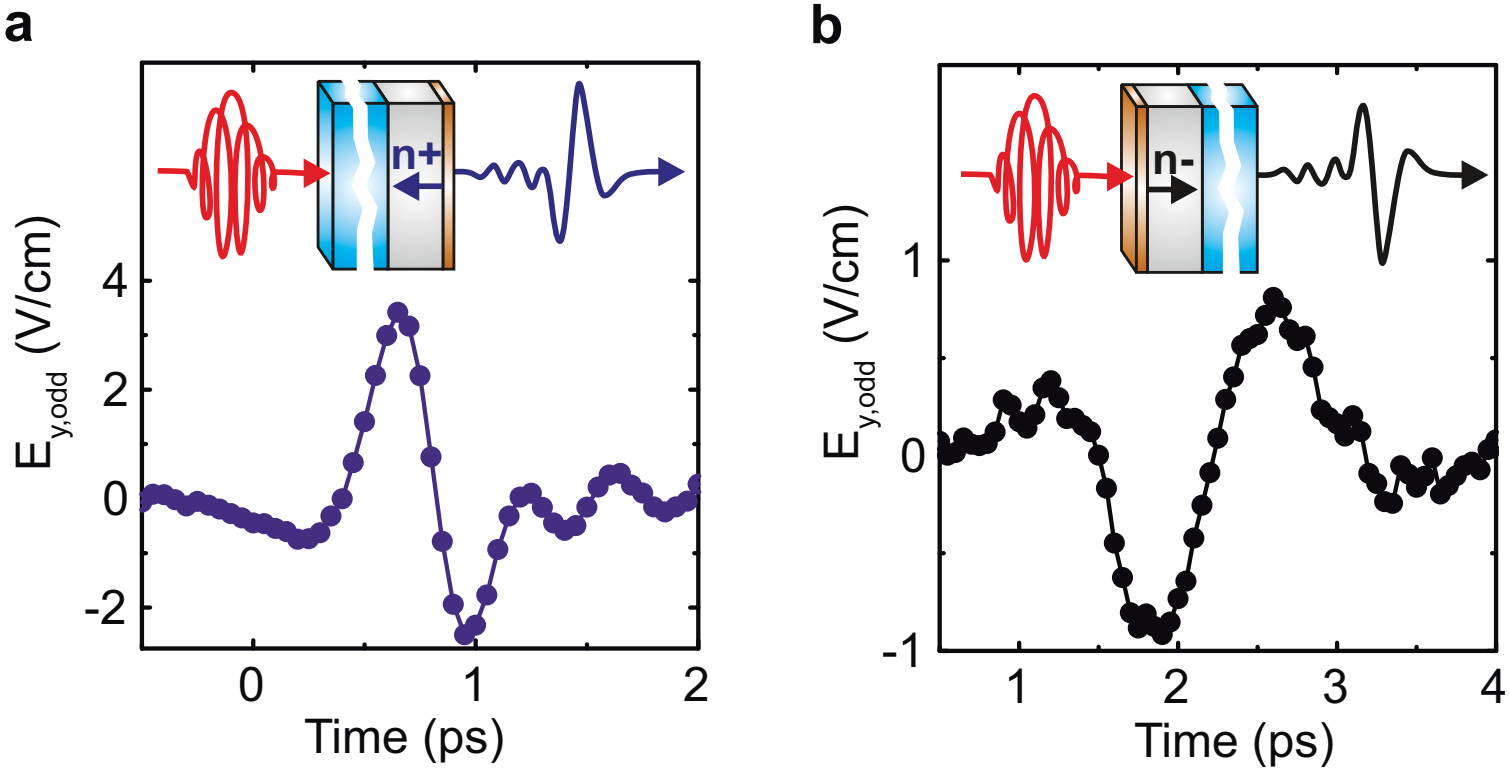
a
b
n+
n-
$E_{y,odd}$ (V/cm)
Time (ps)
4
2
0
-2
1
-1
1
2
3
4

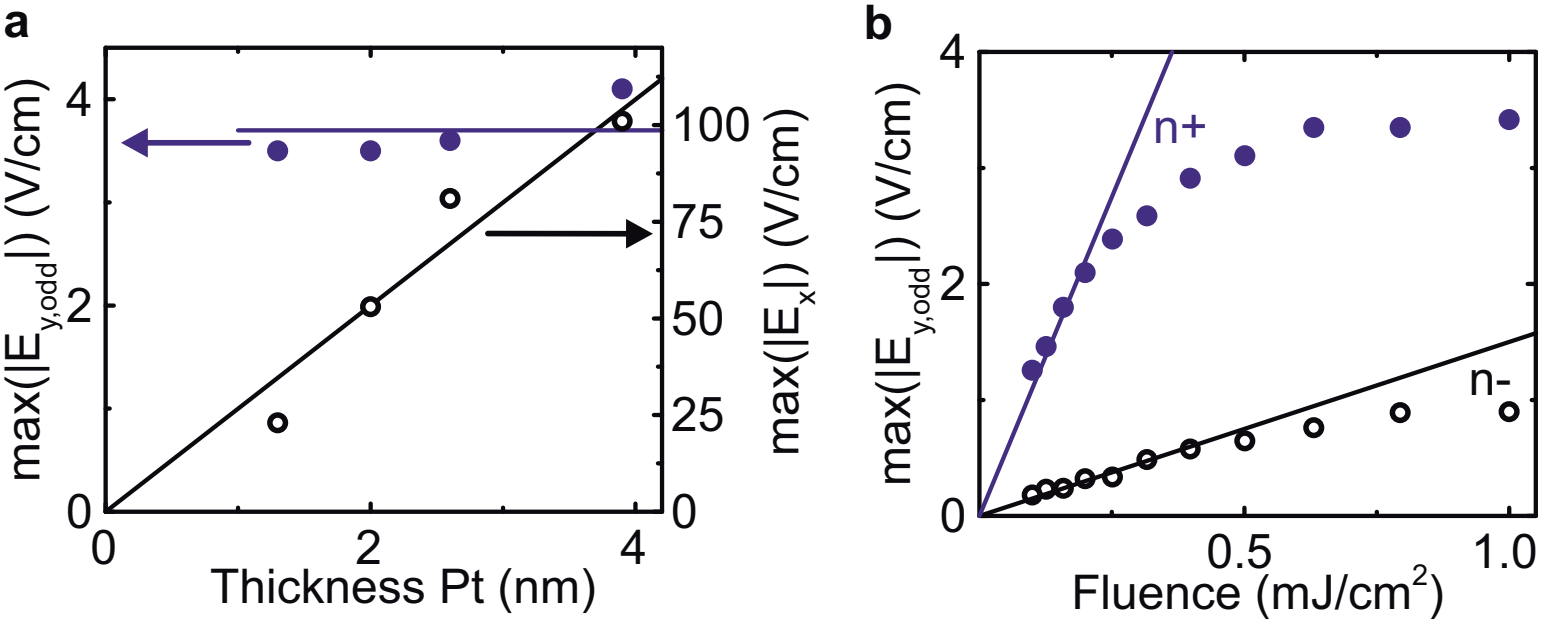
a
b
max(|E_y,odd|) (V/cm)
max(|E_x|) (V/cm)
Thickness Pt (nm)
Fluence (mJ/cm²)
n+
n-
0
2
4
25
50
75
100
0.5
1.0